Available online at www.sciencedirect.com
SCIENCE DIRECT®
Journal of Magnetic Resonance 172 (2005) 242–253
JMR Journal of Magnetic Resonance
www.elsevier.com/locate/jmr

A simulation algorithm based on Bloch equations and product operator matrix: application to dipolar and scalar couplings

Congbo Cai[a], Zhong Chen[a,b,*], Shuhui Cai[a], Jianhui Zhong[b,*]

[a] Department of Physics, State Key Laboratory of Physical Chemistry of Solid Surface, Xiamen University, Xiamen, Fujian 361005, PR China
[b] Departments of Radiology and Physics and Astronomy, University of Rochester, Rochester, NY 14642, USA

Received 19 July 2004; revised 22 October 2004
Available online 21 November 2004

Abstract

A product operator matrix is proposed to describe scalar couplings in liquid NMR. Combination of the product operator matrix and non-linear Bloch equations is employed to describe effects of chemical shift, translational diffusion, dipolar field, radiation damping, and relaxation in multiple spin systems with both scalar and dipolar couplings. A new simulation algorithm based on this approach is used to simulate NMR signals from dipolar field effects in the presence of scalar couplings. Several typical coupled spin systems with both intra-molecular scalar couplings and inter-molecular dipolar couplings are simulated. Monte Carlo methods are incorporated into simulations as well to analyze diffusion process in these complicated spin systems. The simulated results of diffusion and relaxation parameters and 2D NMR spectra are coincident with the experimental measurements, and agree with theoretical predictions as well. The simulation algorithm presented herein therefore provides a convenient means for designing pulse sequences and quantifying experimental results in complex coupled spin systems.

Keywords: NMR; Monte Carlo simulation; Inter-molecular MQC; Intra-molecular MQC; Dipolar couplings; Scalar couplings

1. Introduction

In 1946, soon after the experimental discovery of magnetic resonance, Bloch formulated a set of phenomenological motion equations for various magnetization components [1]. These equations have played a central role in elucidating magnetic resonance phenomena ever since [2]. In 1956, Torrey modified the Bloch equation by incorporating a diffusion term [3]. Dynamics of an ensemble of spins without mutual couplings is usually well described by the Bloch equations [4,5], which can be viewed as mathematical descriptions of precession of the macroscopic magnetization vector around a (possibly time-dependent) magnetic field. With the Bloch equations, effects of relaxation, molecular diffusion, chemical shift, magnetic field inhomegeneity, radiation damping, and long-range dipolar field can all be incorporated into spin dynamic calculations. However, Bloch equations as a model for magnetization vectors fail when scalar couplings exist in spin systems. The reason is that the scalar coupling is a microscopic quantum effect, which in general cannot be described as precession of three-dimensional macroscopic vectors. In this case, the Bloch equations have to be replaced usually with a more complex description using the density matrix formalism [6]. Though the density matrix formalism can deal with complex quantum-mechanical behaviors of an ensemble of spins, it is difficult to handle macroscopic effects such as radiation damping, diffusion, and long-range dipolar field. Therefore, both of the Bloch equations and density matrix formalism have their own advantages and shortcomings.

Recent studies of high order multiple spin echoes in multiple-pulse NMR, which are signatures of

* Corresponding authors. Fax: +1 585 273 1033 (Z. Chen); +1 585 273 4518 (J. Zhong).
E-mail addresses: chenz@jingxian.xmu.edu.cn (Z. Chen), jianhui.zhong@rochester.edu (J. Zhong).

1090-7807/$ - see front matter © 2004 Elsevier Inc. All rights reserved.
doi:10.1016/j.jmr.2004.11.003

inter-molecular multiple quantum coherences (MQCs) [7,8], have triggered some extensive theoretical and experimental activities [9–12] and resulted in exciting novel applications in MRS and MRI [13,14]. The phenomenon results from long-range dipolar couplings among distant dipoles of abundant spins in liquid. Two superficially quite different theoretical frameworks have emerged to explain the phenomenon. The classical or "mean-field" treatment introduces a dipolar demagnetizing field or distant dipolar field, which produces non-linear terms in the Bloch equations for the magnetization. It has been used in a wide variety of applications [9,10]. Alternatively, in the Warren's treatments of inter-molecular multiple-quantum coherences (referred to as "Warren's treatments" later) the dipolar field is expressed in terms of pair-wise interactions between all the spins in a sample [15]. The observable magnetization is derived from multiple-spin operators in the equilibrium density matrix with the high temperature approximation removed. However, except for some geometrically symmetrical samples with magnetization modulated in one direction only, analytical expressions are mostly unobtainable using the Warren's treatments. In an attempt to take the advantages and overcome shortcomings in both the classical dipolar field treatments and the Warren's treatments, we propose a new algorithm based on a combined use of matrix operations and the Bloch equations, to simulate NMR signals from systems with inter-molecular MQCs in the presence of relaxation, radiation damping, diffusion, and also scalar couplings. The simulated results are verified theoretically and experimentally.

2. Theories and methods

2.1. Dynamical equations for spins

Deville introduced the concept of the classical dipolar field, and proposed the non-linear Bloch equations with dipolar field term [16]. After that, Jeener proposed an iterative scheme for solving the "modified Bloch-Redfield equations" [10]. If the superscript i represents the ith type of spins, the motion equation of the magnetization vector $\boldsymbol{M}^{(i)}(\boldsymbol{r},t)$ in a frame rotating at the Larmor frequency is given by:

$$\begin{aligned}\frac{\mathrm{d}\boldsymbol{M}^{(i)}(\boldsymbol{r},t)}{\mathrm{d}t} &= \gamma\boldsymbol{M}^{(i)}(\boldsymbol{r},t)\left\{\frac{\omega_i}{\gamma}\hat{\boldsymbol{z}} + \boldsymbol{G}(\hat{\boldsymbol{s}},\boldsymbol{r})z + \Delta\boldsymbol{B}(\boldsymbol{r},t) \right.\\ &\left. + \sum_j\left[\boldsymbol{B}_r^{(j)}(\boldsymbol{r},t) + \boldsymbol{B}_d^{(j)}(\boldsymbol{r},t)\right]\right\}\\ &- \frac{M_x^{(i)}(\boldsymbol{r},t)\hat{\boldsymbol{x}} - M_y^{(i)}(\boldsymbol{r},t)\hat{\boldsymbol{y}}}{T_2^{(i)}(\boldsymbol{r})} + \frac{M_0^{(i)}\hat{\boldsymbol{z}} - M_z^{(i)}(\boldsymbol{r},t)\hat{\boldsymbol{z}}}{T_1^{(i)}(\boldsymbol{r})}\\ &+ D_T^{(i)}\nabla^2\boldsymbol{M}^{(i)}(\boldsymbol{r},t), \end{aligned} \tag{1}$$

where γ is the magnetogyric ratio; $\hat{\boldsymbol{x}}$, $\hat{\boldsymbol{y}}$, and $\hat{\boldsymbol{z}}$ are unit vectors along three orthogonal coordinate axes; $\hat{\boldsymbol{s}}$ is a unit vector along the direction of the gradient applied for modulating the dipolar field, and $G(\hat{\boldsymbol{s}},\boldsymbol{r})$ is the strength of this gradient along the $\hat{\boldsymbol{s}}$ direction at the position $\boldsymbol{r}$; $\Delta\boldsymbol{B}(\boldsymbol{r},t)$ is the inhomogeneous field at the position $\boldsymbol{r}$; $D_T^{(i)}$ is the translational self-diffusion coefficient of the ith type of spins; $T_1^{(i)}$ and $T_2^{(i)}$ are longitudinal and transverse relaxation times of the ith type of spins, respectively. $\boldsymbol{M}^{(i)}(\boldsymbol{r},0) = M_0^{(i)}\hat{\boldsymbol{z}}$ is the initial magnetization vector of the ith type of spins. Generally, modulation in magnetization can be introduced by pulsed gradient fields, spatial variation in the magnetization density, and inhomogeneity in the static magnetic field. The vector $\hat{\boldsymbol{s}}$ is, therefore, not always along $\hat{\boldsymbol{z}}$ even when the gradient is applied along this direction. However, in most solution NMR, all other factors are much weaker compared to pulse gradient fields which are applied to modulate the magnetization, so it is assumed that $\hat{\boldsymbol{s}}$ is along the $\boldsymbol{z}$ direction for simplification in the following simulation. $\boldsymbol{B}_r^{(j)}(\boldsymbol{r},t)$ is the radiation damping field given by [17]:

$$\boldsymbol{B}_r^{(j)}(\boldsymbol{r},t) = \frac{\langle M_y^{(j)}(t)\rangle}{\gamma M_0^{(j)}\tau_r^{(j)}}\hat{\boldsymbol{x}} + \frac{\langle M_x^{(j)}(t)\rangle}{\gamma M_0^{(j)}\tau_r^{(j)}}\hat{\boldsymbol{y}}, \tag{2}$$

where $\tau_r^{(j)} = 1/(2\pi\eta M_0^{(j)}Q\gamma)$ is the characteristic time of radiation damping, η is the filling factor, Q is the probe Q-factor, and $\langle M_x^{(j)}(t)\rangle$ and $\langle M_y^{(j)}(t)\rangle$ are the average magnetizations in the transverse plane.

$\boldsymbol{B}_d^{(j)}(\boldsymbol{r},t)$ is the dipolar field in position $\boldsymbol{r}$ at time t, produced by the jth type of spins due to effect of dipolar interactions in a concentrated sample. It is the only part survived averaging from the Zeeman interactions. When the static field B_0 and the equilibrium magnetization distribution $M_0^{(j)}$ satisfy the condition $B_0 \gg \mu_0 M_0^{(j)}$ over the whole sample, $\boldsymbol{B}_d^{(j)}(\boldsymbol{r},t)$ is given by [17]:

$$\begin{aligned}\boldsymbol{B}_d^{(j)}(\boldsymbol{r},t) = \frac{\mu_0}{4\pi}\int \mathrm{d}^3\boldsymbol{r}'\frac{1-3\cos^2\theta_{rr'}}{2|\boldsymbol{r}-\boldsymbol{r}'|^3}[3M_z^{(j)}(\boldsymbol{r}',t)\hat{\boldsymbol{z}}\\ - \boldsymbol{M}^{(j)}(\boldsymbol{r}',t)],\end{aligned} \tag{3}$$

where μ_0 is vacuum magnetic permeability and $\theta_{rr'}$ is the angle between the inter-nuclear vectors connecting spins at positions $\boldsymbol{r}$ and $\boldsymbol{r}'$.

Since the dipolar field is a non-local function of the magnetization and must be integrated over the whole sample for every point in space, it is quite computationally expensive to calculate the dipolar field directly with Eq. (3). In experiments, the magnetization is usually assumed to be fully modulated and vary only in one direction. When a strong linear field is applied in a specific direction $\hat{\boldsymbol{s}}$, a Fourier analysis can show that the non-local dipolar field is reduced into the following form [17]:

$$\boldsymbol{B}_d^{(j)}(\boldsymbol{s},t) = \mu_0\Delta_s[M_z^{(j)}(\boldsymbol{s},t)\hat{\boldsymbol{z}} - \tfrac{1}{3}\boldsymbol{M}^{(j)}(\boldsymbol{s},t)], \tag{4}$$

where $\Delta_s = [3(\hat{\boldsymbol{s}} \cdot \hat{\boldsymbol{z}})^2 - 1]/2$. When $\hat{\boldsymbol{s}}$ is along the $\hat{\boldsymbol{z}}$ direction, we have

$$\boldsymbol{B}_d^{(j)}(\boldsymbol{r},t) = \mu_0[M_z^{(j)}(\boldsymbol{r},t)\hat{\boldsymbol{z}} - \tfrac{1}{3}\boldsymbol{M}^{(j)}(\boldsymbol{r},t)]. \tag{5}$$

If the dipolar field cannot be localized, for example, when the magnetization is not fully modulated or it does not vary only in one direction, a spatial Fourier transform can be used to simplify the relation between $\boldsymbol{B}_d^{(j)}(\boldsymbol{r},t)$ and $\boldsymbol{M}^{(j)}(\boldsymbol{r},t)$:

$$\boldsymbol{B}_d^{(j)}(\boldsymbol{k},t) = \frac{\mu_0}{6}\left[3(\hat{\boldsymbol{k}} \cdot \hat{\boldsymbol{z}})^2 - 1\right]\left\{3M_z^{(j)}(\boldsymbol{k},t)\hat{\boldsymbol{z}} - \boldsymbol{M}^{(j)}(\boldsymbol{k},t)\right\}, \tag{6}$$

where $\boldsymbol{k}$ and $\hat{\boldsymbol{k}}$ are the wave vector and corresponding unit vector in the k space, with

$$\boldsymbol{B}_d^{(j)}(\boldsymbol{k},t) = \int \mathrm{d}^3 r \exp(\mathrm{i}\boldsymbol{k} \cdot \boldsymbol{r})\boldsymbol{B}_d^{(j)}(\boldsymbol{r},t), \tag{7a}$$

$$\boldsymbol{M}^{(j)}(\boldsymbol{k},t) = \int \mathrm{d}^3 r \exp(\mathrm{i}\boldsymbol{k} \cdot \boldsymbol{r})\boldsymbol{M}^{(j)}(\boldsymbol{r},t). \tag{7b}$$

A transformation between the real space and Fourier space can reduce the huge computational time for the spatial integral of the dipolar field [17].

When the acquisition time is relatively short, signal attenuation due to diffusion effects can generally be ignored. However, as the observable signal grows over a time of the order of the dipolar demagnetizing time $\tau_d^{(j)} = 1/(\gamma\mu_0 M_0^{(j)})$, it is essential to include the diffusion effect [15]. The diffusion attenuation may be treated in Fourier transformation space. The calculation of the bulk diffusion operator $D_T^{(i)}\nabla^2$ is reduced to multiplication $-D_T^{(i)}k^2$ in the Fourier space. Note that the diffusion operator $D_T^{(i)}\nabla^2$ is only valid for isotropic samples. $\nabla \cdot D_T^{(i)}\nabla$ must be used for anisotropic samples like liquid crystals [18], where $D_T^{(i)}$ is a tensor. Moreover, in the case of "anomalous diffusion," where molecular displacements during successive time intervals are correlated, Torrey's method (diffusion operator $D_T^{(i)}\nabla^2$) does not apply and one has to resort to other methods [19]. Monte Carlo method is a good choice in such case.

Eq. (1) is a set of ordinary differential equations. In order to describe the detected NMR signals at a time t_{final}, Eq. (1) must be integrated from $t = 0$ to t_{final}. This can be done with a fifth-order Cash–Karp Runge–Kutta formulism [17]. The step size during time evolution can be varied based on estimation of the truncation errors and balance between the calculation speed and needed numerical accuracy [20].

2.2. Product operator matrix method

Several works have been carried out to treat strongly coupled spin systems and multiple quantum effects. For example, a treatment of inter-molecular MQCs in the presence of scalar couplings in solution NMR has been discussed by Warren and co-workers [21]. Based on the density matrix, Stables et al. [6] have proposed a method to simulate the effects of scalar couplings in spin echo experiments. Edén has discussed simulations in the solid-state NMR [22], including the spin systems with strongly coupling and spin $> 1/2$. However, these methods are hard to incorporate macroscopic effects such as diffusion and radiation damping in coupled spin systems during multiple-pulse experiments. Jeener [19,23] provided a similar tool to solve the J-coupled spin systems under dipolar effects using spin density matrix. A simple numerical technique was proposed for the prediction of the effects of diffusion in spin echo experiments of the CRAZED type. However, since density matrix in a multiple-spin system such as what is dealt with in this work is complex, the simulation process based on standard density matrix becomes difficult and time-consuming. Recently, Blanton provided a fast NMR C++ tool kit, with which one can simulate macroscopic effects or microscopic effects when they exist independently [24]. Problems emerge, however, when scalar coupling (which is a quantum mechanical effect) needs to be considered together with the effects of dipolar field and radiation damping (which are macroscopic effects). Helgstrand and Allard also distributed a powerful NMR simulation tools (http://www.bpc.lu.se/QSim/index.html). However, the simulation is still divided into two different methods: classical and quantum mechanical, so the situation is not improved. Actually, the macroscopic effects, such as radiation damping, diffusion and dipolar field are not included in their simulation. Since pair-wise spin–spin or multi-spin interactions cannot be represented by magnetization vectors, scalar couplings cannot be introduced into the non-linear Bloch equations directly. To describe the evolution behaviors of scalar couplings in the course of solving the non-linear Bloch equations, we propose to use a product operator matrix, M_{mat}, to describe scalar couplings among multiple spins.

If I and S represent two kinds of spins (either homonuclear or hetero-nuclear) scalarly coupled with each other in one molecule, a product operator matrix for an I_nS_m spin-1/2 system can be built with a $\underbrace{4 \times 4 \times \cdots \times 4}_{n+m}$ matrix, where n and m are the numbers of I and S spins, respectively. Its element number is the same as that of the density operator matrix ($2^{n+m} \times 2^{n+m}$ matrix). In the simulation, the sample is always divided into some cells, for example, along the z axis. Every cell is represented by a matrix containing the complete spin information of the cell at the corresponding position. Therefore, a matrix can represent not only a coupled spin system in one molecule, but also represent the average spin property of one cell. Element of the product operator matrix is represented by $M_{\mathrm{mat}}(I_{1a}, I_{2a}, \ldots, I_{ia}, \ldots, I_{n+m,a})$, where the symbol I_{ia} represents a specific component (such as I_{ix}, I_{iy}, or

I_{iz}) of the ith spin operator or unit element E. Since the base operator, $2^{q-1}I_{1a}I_{2a}\cdots I_{na}S_{1a}S_{2a}\cdots S_{ma}$, corresponds to a coherence term, where q is the number of spin operators in the product operator, $M_{\mathrm{mat}}(I_{1a}, I_{2a}, \ldots, I_{ia}, \ldots, I_{n+m,a})$ can be considered as the magnitude of the base operator. For example, $M_{\mathrm{mat}}(I_{1x}, I_{2x}, \ldots, I_{nx}, S_{1x}, \ldots, S_{mx})$, $M_{\mathrm{mat}}(I_{1y}, I_{2x}, \ldots, I_{nx}, S_{1x}, \ldots, S_{mx})$, $M_{\mathrm{mat}}(I_{1z}, I_{2x}, \ldots, I_{nx}, S_{1x}, \ldots, S_{mx})$, and $M_{\mathrm{mat}}(E, I_{2x}, \ldots, I_{nx}, S_{1x}, \ldots, S_{mx})$ represent the magnitude of coherence terms $2^{n+m-1}I_{1x}I_{2x}\cdots I_{nx}S_{1x}S_{2x}\cdots S_{mx}$, $2^{n+m-1}I_{1y}I_{2x}\cdots I_{nx}S_{1x}S_{2x}\cdots S_{mx}$, $2^{n+m-1}I_{1z}I_{2x}\cdots I_{nx}S_{1x}S_{2x}\cdots S_{mx}$, and $2^{n+m-2}I_{2x}I_{3x}\cdots I_{nx}S_{1x}S_{2x}\cdots S_{mx}$, respectively. $M_{\mathrm{mat}}(I_{1x}, E, \ldots, E, \ldots, E)$ represents the intensity value of I_{1x} term, which is a single-spin term for the x component of the I_1 spin. Similarly, I_{ix}, I_{iy}, I_{iz}, S_{jx}, S_{jy}, and S_{jz} represent the corresponding components of the spin operators I_i or S_j. The elements of the product operator matrix corresponding to I_{ix}, I_{iy}, and I_{iz} (or S_{jx}, S_{jy}, and S_{jz}) can be treated as specific components of a general "magnetization vector" $\boldsymbol{M}^{(i)}$. In fact, they are considered to account for the magnetization in the volume element at a specific position of the sample. The evolution of $\boldsymbol{M}^{(i)}$ under chemical shift, RF field, inhomogeneous background field, dipolar field, radiation damping, and diffusion can be described by the modified Bloch equations shown in Eq. (1). Relaxation is not included except for the single-quantum term due to the complexity of relaxation in the case of the intra-molecular MQCs [25]. Scalar couplings are introduced independently into the product operator matrix. According to the rules of scalar couplings, there exist only $2I_{iz}S_{jz}(1 \leqslant i \leqslant n,\ 1 \leqslant j \leqslant m)$ evolution operators for an I_nS_m spin system [26]. Matrix operation rules for the scalar coupling operator, $2I_{iz}S_{jz}$, can therefore be deduced:

$$\left.\begin{array}{c} M_{\mathrm{mat}}(I_{1a}, I_{2a}, \ldots, E, \ldots, I_{na}, S_{1a}, S_{2a}, \ldots, S_{jx}, \ldots, S_{ma}) \overset{2I_{iz}S_{jz}}{\longleftrightarrow} \\ M_{\mathrm{mat}}(I_{1a}, I_{2a}, \ldots, I_{iz}, \ldots, I_{na}, S_{1a}, S_{2a}, \ldots, S_{jy}, \ldots, S_{ma}) \\ M_{\mathrm{mat}}(I_{1a}, I_{2a}, \ldots, E, \ldots, I_{na}, S_{1a}, S_{2a}, \ldots, S_{jy}, \ldots, S_{ma}) \overset{2I_{iz}S_{jz}}{\longleftrightarrow} \\ M_{\mathrm{mat}}(I_{1a}, I_{2a}, \ldots, I_{iz}, \ldots, I_{na}, S_{1a}, S_{2a}, \ldots, S_{jx}, \ldots, S_{ma}) \end{array}\right\} \tag{8}$$

Eq. (8) provides evolution relations of the matrix elements due to the scalar coupling operator $2I_{iz}S_{jz}$ in the product operator matrix. The relations are simplified by:

$$\left.\begin{array}{l} aS_{xj} + bI_{zi}S_{yj} \overset{\theta 2I_{zi}S_{zj}}{\underset{\theta=\pi J}{\longrightarrow}} aS_{xj}\cos\theta + aI_{zi}S_{yj}\sin\theta + bI_{zi}S_{yj}\cos\theta - bS_{xj}\sin\theta \\ aS_{yj} + bI_{zi}S_{xj} \overset{\theta 2I_{zi}S_{zj}}{\underset{\theta=\pi J}{\longrightarrow}} aS_{yj}\cos\theta - aI_{zi}S_{xj}\sin\theta + bI_{zi}S_{xj}\cos\theta + bS_{yj}\sin\theta \end{array}\right\}, \tag{9}$$

where a and b are the coefficients of the corresponding terms, J is the scalar coupling constant of the spin system I_nS_m, and τ is the step size used in the Cash–Karp Runge–Kutta equation [17]. In Eq. (9), all terms irrelevant to the evolution under the operator $2I_{iz}S_{jz}$ were ignored. After every evolution, the corresponding scalar coupling process is calculated. For other spin coupled systems, similar product operator matrix and scalar coupling rules are easily obtained.

2.3. Monte Carlo method

Numerical simulation is very powerful in handling some complicated systems in which spin dynamics and time evolution are very difficult to follow with analytical methods alone [27–29]. For example, Monte Carlo method can be used to simulate free and restricted diffusion through Brownian motion. A common way to simulate such diffusion process is to represent diffusion as a sequence of small random displacements

$$Z(t+\tau) = Z(t) + \Delta Z, \tag{10}$$

where $Z(t)$ is the position of the particle at time t, $Z(t+\tau)$ is its position at time $t+\tau$, and ΔZ is a random displacement of the particle in the time interval τ. Because we limit our discussion to the situation in which the magnetic gradient is applied only along the z direction, only the displacement along this direction needs to be considered. Since the motion of particles is stochastic, the displacement ΔZ can be given by random walk with $\Delta Z = \sqrt{2D_T\tau}\varepsilon\cos(\beta)$, where β is the angle between the z axis and the walking direction of the simulated particle, and ε is a random number. If the average free path, λ, is set to $\sqrt{2D_T\tau}$, the free path distribution sampling method is then represented by [30]:

$$\varepsilon = -\ln(\varepsilon_1), \tag{11}$$

where both ε_1 and β are uniformly distributed and can be generated by a computer random number generator directly (with ε_1 limited between 0 and 1, and β limited between 0 and 2π). The random number ε is completely uncorrelated, i.e., its self-correlation coefficient is zero. They are distributed according to the free path distribution function:

$$p(\varepsilon) = \mathrm{e}^{-\varepsilon/\lambda}. \tag{12}$$

Though diffusion is usually considered to be free in solution NMR, a finite boundary is needed for simulation. We assume that the length of the sample is $L = 2R$, and perfectly reflecting walls are located at $z = -R$ and $z = R$. The reflecting boundary condition is accounted for by replacing z with $-z - 2R$, or $2R - z$ whenever $z < -R$ or $z > R$. In the simulation, R of several mm is used, and the diffusion is taken to be free between boundaries. Although the diffusion term in the non-linear Bloch equations can describe diffusion behavior generally, Monte Carlo method is more flexible and intuitive in the cases of restricted diffusion.

2.4. Simulation process

The simulation procedure was divided into two steps. First, a Monte Carlo method was employed to simulate the diffusion process of spins. Second, the dipolar field was calculated after every spin was moved to a new position after each step of motion, and then the spin evolution based on the non-linear Bloch equations was calculated. This process was repeated till the end of sampling. Parameters used in simulations vary with the different spin systems. Details will be given in the following section, when simulation results are discussed.

3. Results and discussion

3.1. Simulation of diffusion effects

Self-diffusion is a process of random translational motion of molecules driven by internal kinetic energy. Diffusion NMR spectroscopy and MR imaging are presently the only available non-invasive methods that can provide information about molecular displacements in a spatial scale comparable to cell dimensions of biological systems [31]. The mathematics required for describing diffusion is rather complicated except for diffusion in free space or restricted diffusion within samples of simple geometries. As a result, analytical solutions are generally impossible and numerical solutions are called for [15]. The diffusion behavior under the dipolar field has been discussed previously [12,32–34]. However, to the best of our knowledge, it has not been simulated with the combination of the dipolar field model and Monte Carlo methods. In addition, the diffusion behavior of inter-molecular MQCs in the presence of scalar couplings has not been reported either.

The Monte Carlo method with a random walk model can be used to describe molecular diffusion process, and non-linear Bloch equations and product operator matrix method depict time evolution of each spin under chemical shift, dipolar field, relaxation, and scalar coupling. Therefore, diffusion process on conventional single-quantum coherences (SQCs), intra-molecular double-quantum coherences (DQCs), and inter-molecular DQCs can be studied by combining Monte Carlo method with non-linear Bloch equations and product operator matrix method. In this section, we focus on the diffusion behaviors under the joint effects of the dipolar field and intra-molecular scalar couplings.

Field gradients applied during spin evolution (either for dipolar field modulation or for diffusion measurements) attenuate NMR signal. When the pulse sequences shown in Figs. 1A and B are employed, diffusion attenuation factor E due to free diffusion is given by:

$$\ln E = -\gamma^2 G_1^2 \delta^2 D_T^{\mathrm{App}} (\Delta_1 + 2\delta/3), \tag{13}$$

where D_T^{App} is the apparent diffusion coefficient, δ and G_1 are the duration and amplitude of diffusion weighting gradients, and Δ_1 is the time interval between the two diffusion weighting gradients.

As an example, a two-component $AX + C$ spin system with different resonance offsets was simulated for diffusion effects in multiple-spin systems with intra- and inter-molecular couplings. AX denotes solute with $J_{AX} = 10$ Hz and C denotes solvent. Their resonance offsets were set to be $\omega_A = 400$ Hz, $\omega_X = -300$ Hz, and $\omega_C = 0$ Hz, respectively. It is assumed that the self-diffusion rates of C and AX components are 2.5×10^{-9} m^2/s

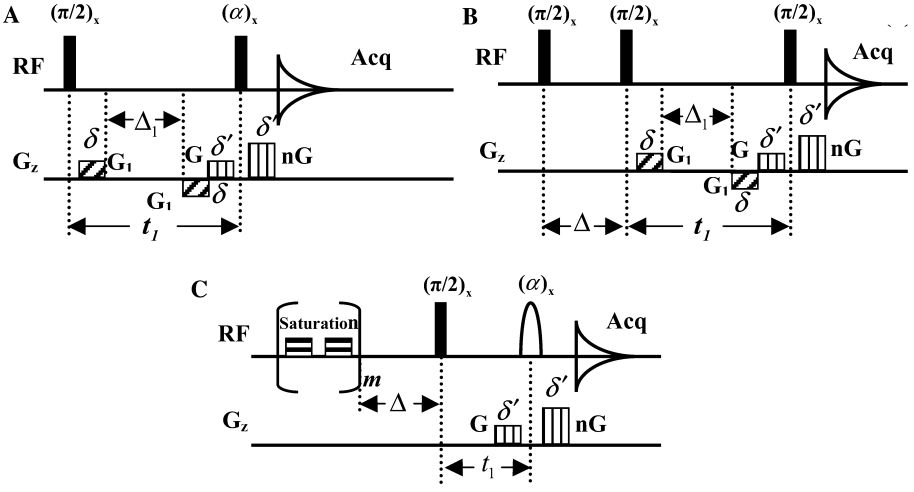

Fig. 1. Pulse sequences used in this paper: (A) a modified CRAZED sequence for characterization of SQCs and inter-molecular MQCs, (B) a modified intra-molecular MQC sequence for characterization of MQCs, and (C) a modified CRAZED sequence for characterizing longitudinal relaxation of SQCs and inter-molecular DQCs.

and 1.5×10^{-9} m^2/s, respectively. These parameters are close to what have been measured in experiments. Other parameters used in the simulation are: longitudinal and transverse relaxation times of the three peaks are all 1.0 s; duration of all gradient pulses is 2 ms; acquisition time of free induced decay signal is 1.64 s with 4096 sampling points. The length of the sample is 1.0×10^{-3} m along the z axis. The number of the particles is 4×10^5, and the longitudinal axis is divided into 1000 units. The step size for the Monte Carlo simulation is 0.4 ms. The pulse sequence shown in Fig. 1A with $\alpha = 0$ and $G = 0$ is used for simulation of conventional SQC diffusion, and with $\alpha = \pi/2$ and $n = -2$ for simulation of inter-molecular DQC diffusion effects. The pulse sequence shown in Fig. 1B is used for simulation of intra-molecular DQC diffusion effects. In inter- and intra-molecular DQC simulations, the amplitude of the coherence-selection gradient G is 10 G/cm. The amplitude of diffusion weighting gradients G_1 is varied from 0 to 9 G/cm with increment of 1 G/cm. If the second RF pulse in Fig. 1A were not frequency selective for inter-molecular DQCs, the signals located at the solute peak positions in the 1D spectrum would not only come from the solvent–solute coherence signal, but also come from the solute–solute coherence signal. It is then impossible to obtain the apparent diffusion rate of a specific component. Therefore, the second RF pulse in Fig. 1A is set to be selective only for the solvent (i.e., C component) to eliminate the solute–solute coherence peaks. Simulated diffusion rates from different coherence orders during the evolution period are listed in Table 1. The simulated SQC diffusion rates, $D^C_{\mathrm{SQC}} = (2.47 \pm 0.01) \times 10^{-9}$ m^2/s and $D^{AX}_{\mathrm{SQC}} = (1.49 \pm 0.01) \times 10^{-9}$ m^2/s, are very close to their input values. According to the diffusion properties in a homo-nuclear experiment [35], the signals originating from intra-molecular MQCs would decay exponentially at a rate $D_{\mathrm{MQC}} = n^2 D_T$ [36]. For intra-molecular DQCs, the simulated apparent diffusion rate of the solute is found to be $D^{AX}_{\mathrm{DQC}} = (5.90 \pm 0.01) \times 10^{-9}$ m^2/s, coincident with the theoretical prediction value of 6.0×10^{-9} m^2/s. For inter-molecular DQCs, our previous work [12] has demonstrated the following relationship: $D^{AX,C}_{\mathrm{iDQC}} = D^C_T + D^{AX}_T$ and $D^{C,C}_{\mathrm{iDQC}} = 2D^C_T$, where $D^{AX,C}_{\mathrm{iDQC}}$ denotes the apparent diffusion rate of the signal originating from the solute–solvent inter-molecular DQCs, and $D^{C,C}_{\mathrm{iDQC}}$ represents the apparent diffusion rate of the signal originating from solvent–solvent inter-molecular DQCs.

Table 1
Diffusion rates of $AX + C$ spin system

Diffusion rate	Simulation result ($\times 10^{-9}$ m^2/s)	Theoretical prediction ($\times 10^{-9}$ m^2/s)
D^C_{SQC}	2.47 ± 0.01	2.50
D^{AX}_{SQC}	1.49 ± 0.01	1.50
Intra-molecular D^{AX}_{DQC}	5.90 ± 0.01	6.00
Inter-molecular $D^{C,C}_{\mathrm{iDQC}}$	5.01 ± 0.05	5.00
Inter-molecular $D^{AX,C}_{\mathrm{iDQC}}$	3.99 ± 0.02	4.00

In Table 1, the simulated diffusion rates are $D^{C,C}_{\mathrm{iDQC}} = (5.01 \pm 0.05) \times 10^{-9}$ m^2/s and $D^{AX,C}_{\mathrm{iDQC}} = (3.99 \pm 0.02) \times 10^{-9}$ m^2/s, respectively, in good agreement with the theoretical predictions of 5.0×10^{-9} m^2/s and 4.0×10^{-9} m^2/s, respectively. These results suggest that the combination of Monte Carlo method, non-linear Bloch equations, and the product operator matrix method can be used successfully to simulate diffusion under complex pulse sequences and with both intra- and inter-molecular MQC effects.

3.2. Simulation of relaxation effects

Transverse relaxation process of nuclear systems is related to rotational motion and transport of molecules, molecular structure, and spin–spin interactions. The apparent transverse relaxation time of n-order inter-molecular dipolar interactions, $T^{\mathrm{App}}_{2,n}$, may contain information to complement conventional SQC T_2 measurements [37]. Transverse relaxation behaviors of SQCs and inter-molecular DQCs were simulated for a two-component spin system, consisting of I (solvent) and S (solute) spins with different chemical shifts and relaxation times. This system mimics the real spin systems we studied previously [12]. The simulation parameters are $\omega_I = 0$ Hz (solvent), $\omega_S = 400$ Hz (solute), $T^I_1 = 2.0$ s, $T^I_2 = 1.0$ s, $T^S_1 = 1.0$ s, and $T^S_2 = 0.6$ s. Diffusion rates of both the solvent and solute are 2.0×10^{-9} m^2/s. The pulse sequence shown in Fig. 1A with $G_1 = G = 0$ and $\alpha = 0$ is used for conventional SQC simulation, and with $G_1 = 0$, $n = -2$, and $\alpha = \pi/2$ for inter-molecular DQC simulation. The second RF pulse is selective for spin I in inter-molecular DQC simulation. Δ_1 is varied from 0 to 0.45 s with increment of 0.05 s. Other simulation parameters are the same as those in Section 3.1.

The transverse relaxation attenuation equation is [37]:

$$\ln E = -\Delta_1 / T^{\mathrm{App}}_2, \tag{14}$$

where T^{App}_2 is the apparent transverse relaxation time. The simulation results are listed in Table 2. The apparent transverse relaxation time of inter-molecular DQC signal ($n = 2$) obeys the following rule [12,38]:

$$1/T^{I,S}_{2,2} = 1/T^I_2 + 1/T^S_2. \tag{15}$$

When the signal is from the solvent–solvent DQCs, the simulated transverse relaxation time is $T^{I,I}_{2,2} = (0.51 \pm 0.01)$ s, in agreement with the theoretical prediction of 0.50 s. When the signal is from the solvent–solute DQCs, its transverse relaxation time $T^{I,S}_{2,2} = (0.38 \pm 0.01)$ s, also coincident with the theoretical value of 0.38 s.

Table 2
Transverse relaxation times of $I + S$ spin system

Transverse relaxation time	Simulation result (s)	Theoretical prediction (s)
SQC T_2^I	0.99 ± 0.01	1.00
SQC T_2^S	0.60 ± 0.01	0.60
Inter-molecular DQC $T_{2,2}^{I,I}$	0.51 ± 0.01	0.50
Inter-molecular DQC $T_{2,2}^{I,S}$ of S	0.38 ± 0.01	0.38

Longitudinal relaxation is a recovery process of longitudinal magnetization from a non-equilibrium state toward the equilibrium state. The saturation-recovery method shown in Fig. 1C was employed to measure longitudinal relaxation time. The first RF pulse is a pre-saturation pulse. For inter-molecular DQCs, the second RF pulse is selective for solvent (I spin) with $\alpha = \pi/2$ and $n = -2$. For SQCs, $\alpha = 0$ and $G = 0$. The saturation recovery time Δ is varied from 0 to 3.8 s with increment of 0.2 s. The dependence of the normalized SQC signal intensity on saturation recovery time Δ is:

$$E = 1 - e^{-\Delta/T_1^I}. \tag{16a}$$

The dependences of the normalized signal intensities from inter-molecular DQCs on Δ are [12]:

$$E_S = (1 - e^{-\Delta/T_1^I})(1 - e^{-\Delta/T_1^S}), \tag{16b}$$

$$E_I = (1 - e^{-\Delta/T_1^I})^2. \tag{16c}$$

Eqs. (16b) and (16c) corresponds to the signals of the solute and solvent, respectively. The simulated results are shown in Fig. 2. Fitting to Eq. (16a) yields the SQC longitudinal relaxation times of (0.99 ± 0.01) s and (1.99 ± 0.01) s for the solute and solvent, respectively. Similarly, the simulated longitudinal relaxation times of the signals from inter-molecular DQCs are (0.99 ± 0.01) s and (1.97 ± 0.01) s for the solute and solvent, respectively. All these results are close to the theoretical values of 1.0 and 2.0 s as calculated with Eqs. (16b) and (16c).

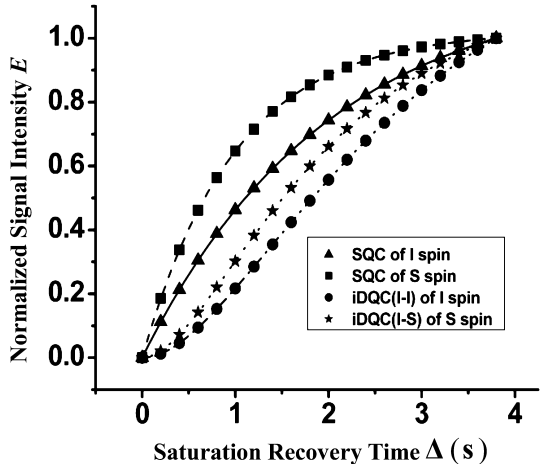

Fig. 2. Normalized longitudinal relaxation curves of a two-component spin system for SQCs and inter-molecular DQCs. The evolution time Δ is from 0 to 3.8 s with increment of 0.2 s. The other simulation parameters are described in context.

3.3. Simulation of 2D spectra of intra- and inter-molecular MQCs

2D spectra of intra- and inter-molecular DQCs and ZQCs were simulated, and the experimental measurements were performed for validation. Since the multiple quantum terms in the product operator matrix do not affect the transverse magnetization in the detection period, they were ignored in the simulation. The sample used for intra- and inter-molecular DQCs and ZQCs studies was a A_2X_3 system with $\omega_A = 400$ Hz and $\omega_X = -518$ Hz, and $J_{AX} = 7.4$ Hz, corresponding to a solution of CH_3CH_2Br in $CDCl_3$ used in measurements at 11.7 T. In the simulation, 1024 points are sampled in the direct detection dimension (F2) with 512 increments in the indirect dimension (F1). Both dimensions are zero-filled to 4096 points. This reduces computational time greatly. It takes about 4 h of CPU time for an A_2X_3 spin system on a PC computer (AMD XP 2500+, 512 Mb memories) to obtain a 2D spectrum with satisfactory signal-to-noise ratio and resolution.

A dilute solution was used in order to eliminate the effects of radiation damping. The pulse sequence shown in Fig. 1B was used for both simulation and measurement. To better reproduce the experimental results, the RF pulses were purposely deviated from the ideal $\pi/2$ pulse by about $\pi/36$ in simulation. Fig. 3 displays the simulated and experimental results of 2D intra-molecular ZQC spectra. Clearly, the simulated spectrum matches the experimental result well. There are totally six cross-peaks in the simulation spectrum. The cross-peaks in the simulated spectrum located at $(\omega_A - \omega_X, \omega_A)$, $(\omega_X - \omega_A, \omega_A)$, and $(0, \omega_X)$ are found correspondingly in the experimental spectrum. The weaker cross-peaks located at $(0, \omega_A)$, $(\omega_A - \omega_X, \omega_X)$, and $(\omega_X - \omega_A, \omega_X)$ are caused by the non-ideal RF pulses and would disappear when the RF pulses are set to be ideal. The regions of the cross-peaks labeled by (I) and (II) are expanded in the figure. It can be seen that cross-peak (I) is a doublet along the F1 axis and a quartet along the F2 axis, and the cross-peak (II) is a singlet along the F1 axis and a triplet along the F2 axis. The multiplicity patterns of the simulated cross-peaks are coincident with the experimental ones quite well. It is worth noting that the experimental conditions were not as ideal as for the theoretical simulation. For example, the effects of radiation damping cannot be eliminated entirely, and the sample may be not pure. These factors lead to some artifacts in experimental spectra, which do not occur in the simulation results.

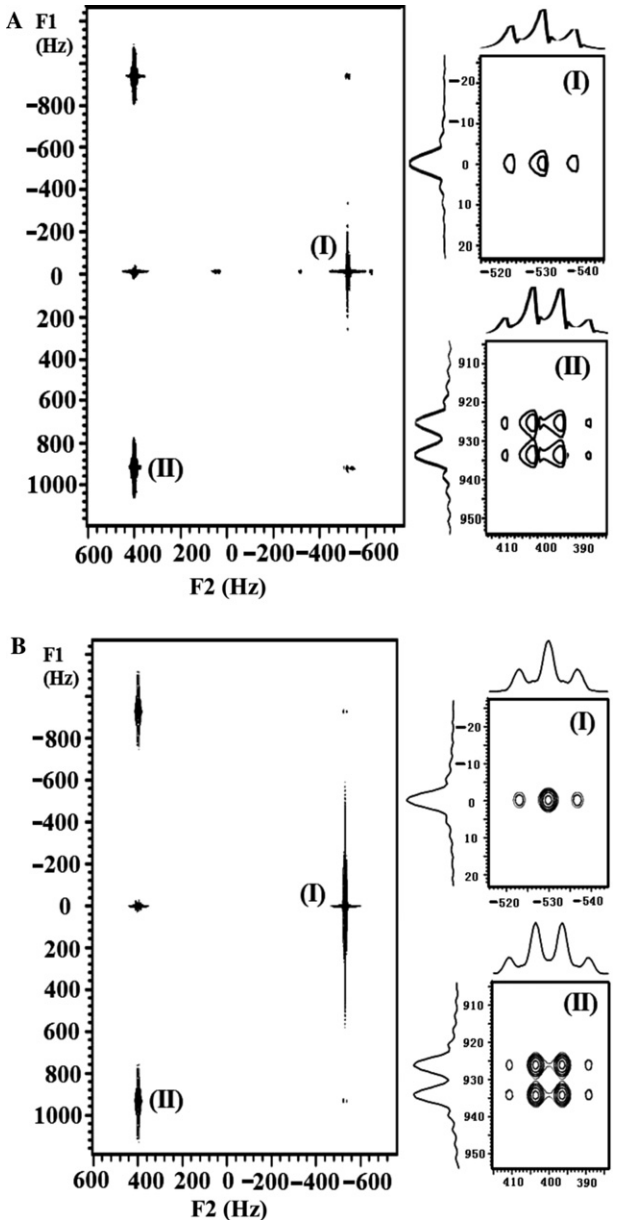

Fig. 3. 2D spectra of intra-molecular ZQCs from experiment (A) and simulation (B). The solute is CH_3CH_2Br denoted as A_2X_3 ($\omega_A = 400$ Hz, $\omega_X = -530$ Hz, and $J_{AX} = 7.4$ Hz), and the solvent is $CDCl_3$. The pulse sequence is shown in Fig. 1B ($n = 0$) where the three RF pulses are deviated from the ideal pulse ($\pi/2$) by about $\pi/36$ in the simulation to better mimic the experimental conditions. The evolution time is $\Delta = 1/2J_{AX}$ to obtain the strongest intra-molecular ZQC signals.

To obtain 2D inter-molecular DQC spectra, the pulse sequence shown in Fig. 1A was applied to a concentrated solution of CH_3CH_2Br in acetone (denoted as $A_2X_3 + C$ with $\omega_A = 691$ Hz, $\omega_X = -227$ Hz, $J_{AX} = 7.4$ Hz, and $\omega_C = 0$ Hz). The probe was detuned to lower Q factor in order to suppress the effects of radiation damping. The simulated and experimental results are shown in Figs. 4 and 5. The second RF pulse is non-selective for spectra in Fig. 4 and selective to acetone for spectra in Fig. 5. Comparing Fig. 4 with Fig. 5, it is clear that the selective RF pulse reduces the number of cross-peaks significantly. Because the inter-molecular solute–solute DQC cross-peaks are eliminated when only the solvent is excited by the second RF pulse, the resultant 2D spectra are greatly simplified. Most interestingly, there exist some "forbidden" cross-peaks such as $(\omega_X + \omega_C, \omega_A)$ and $(\omega_A + \omega_C, \omega_X)$. These "forbidden" cross-peaks arise from competition between inter-molecular dipolar couplings and intra-molecular scalar couplings [39]. Their multiplet patterns are rather different from conventional ones. The regions labeled by (I–IV) are expanded to display more details. Region (I) has a "forbidden" cross-peak which is a doublet along the F1 axis and a quartet along the F2 axis. It is noting that the individual peaks in the quartet have same intensities, quite different from the intensity ratio 1:3:3:1 of a normal quartet. Both simulated and experimental results of the regions labeled by (I–IV) give the same multiplet patterns.

To simulate the effect of non-ideal RF pulses in experiments, flip angles deviated from $\pi/2$ (by about $\pi/36$) were used to simulate the selective inter-molecular DQCs (see Fig. 5). Most simulated cross-peaks find their correspondences in the experimental spectrum. According to the theoretical analysis, there should be only three diagonal peaks (labeled by (I), (II), and (III)) in Fig. 5, corresponding to $(\omega_A + \omega_C, \omega_A)$, $(\omega_X + \omega_C, \omega_X)$, and $(2\omega_C, \omega_C)$. The minor differences between the two spectra may be due to the inhomogeneous broadening of magnetic field, residual effects of radiation damping, non-ideal selective pulse, and non-ideal $(\pi/2)_x$ pulse.

So far, our results suggest that a combination of the product operator matrix operation and non-linear Bloch equations can be employed to follow conveniently and efficiently time evolution processes of complex spin systems with both intra- and inter-molecular couplings under multiple-pulses sequences, which are often difficult or impossible when conventional product operator methods or Bloch equations are applied alone. The results also show that the simulation method presented herein is helpful to identify possible sources of some unexpected experimental results, which may be difficult to identify from theoretical deduction when the spin system is complicated, such as an A_2X_3 system. Different to the non-selective inter-molecular DQC spectra, the cross-peaks in the selective inter-molecular DQC spectra have very simple multiplet patterns (see for example regions (I) and (II) in Fig. 5). Their projections on the F1 axis and F2 axis give the usual SQC 1D spectra.

The product operator matrix is a subset of the density matrix. Since the formalism of conventional density matrix for a multiple-spin system is complicated, the product operator matrix is a good choice for simulation. With physical intuition, the product operator matrix can be operated by the non-linear Bloch equations di-

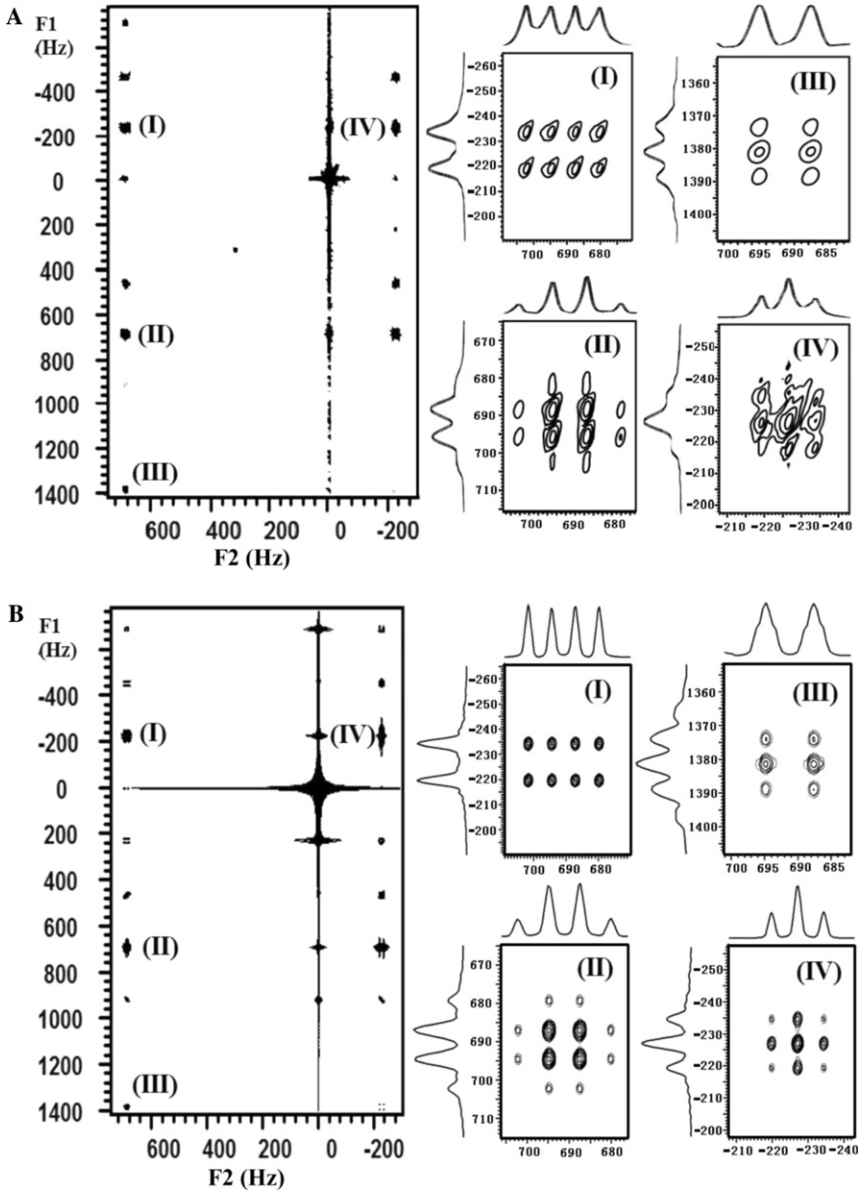

Fig. 4. 2D spectra of non-selective inter-molecular DQCs of the two-component spin system ($A_2X_3 + C$) from experiment (A) and simulation (B). The regions of cross-peaks (I–IV) are expanded. The solute is CH_3CH_2Br (rescaled to $\omega_A = 691$ Hz, $\omega_X = -227$ Hz), and the solvent is acetone ($\omega_C = 0$ Hz). The pulse sequence is shown in Fig. 1A ($n = -2$) with non-selective RF pulses.

rectly. Thus, the effects of the chemical shift and scalar coupling as well as diffusion, relaxation, and dipolar field can be simulated simultaneously. Moreover, the features of standard product operator are reserved in the product operator matrix method. Therefore, this simulation algorithm is simple, efficient and precise even for a complex coupled spin system.

Simulated efficiency is important for a 2D spectrum simulation since a large amount of data need to be calculated. With the simulation algorithm, the computational time for a 2D spectrum is still acceptable. The precision is especially important when self-feedback dynamic exists in the evolution of spin magnetization, such as the radiation damping field or dipolar field. A small calculation error at the beginning of simulation may greatly affect the final results due to a self-feedback process. More explicitness is expected for the chaotic dynamics produced by the joint effect of radiation damping field and dipolar field in the solution NMR due to the high sensitivity of chaos on the initial error. Warren and co-workers have studied the chaotic phenomena in solution NMR [13]. However, they limited their study to the single spin system, since it has been thought that the J coupling cannot be combined with the non-linear Bloch equations. With the product operator matrix approach, it is convenient to extended from single-spin system to complex multiple-spin system with weakly coupling and spin = 1/2 in the study of chaos.

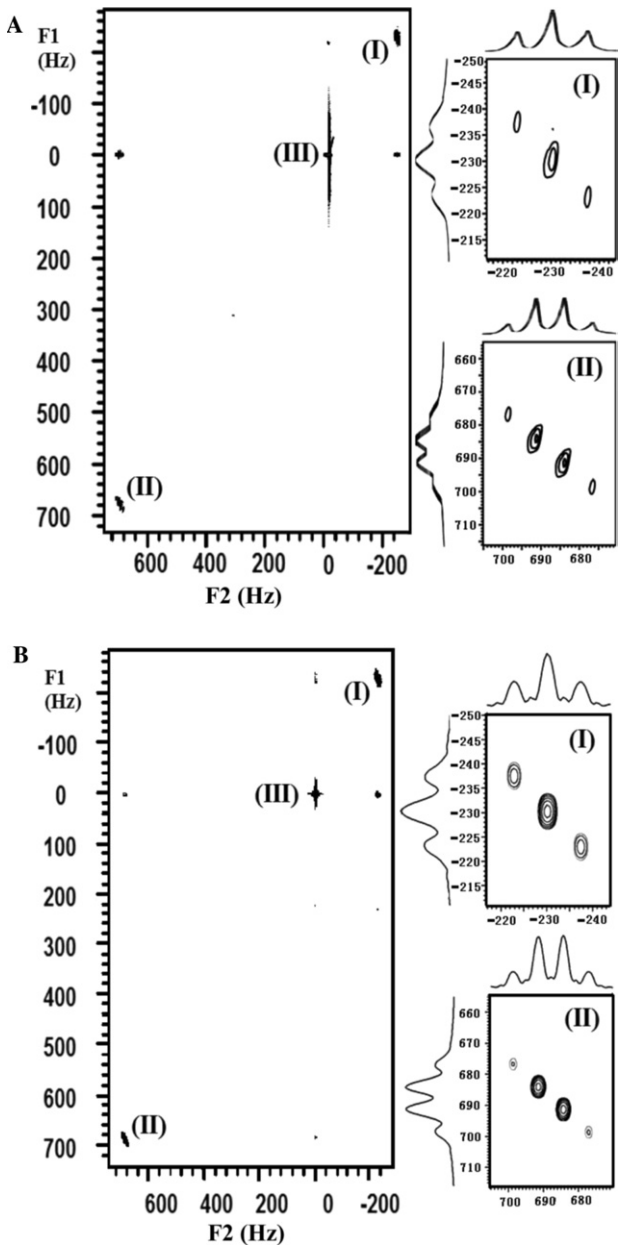

Fig. 5. 2D spectra of selective inter-molecular DQCs of the two-component spin system ($A_2\ X_3 + C$) from experiment and simulation. The regions labeled (I) and (II) are expanded. The pulse sequence is shown in Fig. 1A ($n = -2$) with the second RF pulse selective only for the solvent. The other parameters are the same as in Fig. 4.

It has been shown that the inter-molecular MQCs can provide a new contrast mechanism on MRI [14]. By now all simulations and discussion on inter-molecular MQC MRI are based on single spin system [14,40–42]. Using the simulation method provided herein, more complex spin system with intra-molecular scalar couplings can be studied, and J coupling constant may provide a new important imaging contrast parameter for MRI under inter-molecular MQCs. Further, the efficient algorithm will shorten the MRI simulation time which often takes much computational effect. It is worth noting that the product operator matrix method is only applicable to weakly coupled 1/2 spin systems in solution NMR. For complex spin systems such as strong coupled, spin $> 1/2$ system, and solid-state NMR, the density matrix method is required [23].

The product operator matrix method proposed in this work provides a tool to analyze and simulate simultaneously the effects of chemical shift, J couplings, relaxation, diffusion, dipolar field, and radiation damping. The dipolar field resulted from the CRAZED sequence cannot be ignored in the simulation when a concentrated solution is placed in a strong static magnetic field. Similarly, the radiation damping can be ignored in the simulation only when the probe is detuned and/or the filling factor is very small. For a sample with short T_1 and/or T_2, the relaxation effects cannot be ignored in the simulation. Ignoring the effects of relaxation and diffusion may significantly affect the lineshape of 1D spectra, and may result in errors in the inter-molecular MQCs simulations. On the other hand, the simulated results are coincident with the experimental ones in a dilute sample when the effects of radiation damping and dipolar field are ignored. When both T_1 and T_2 are long enough, the effects of relaxation can also be ignored in the simulation. If the effects of radiation damping, relaxation, and diffusion in the solution NMR can be ignored, the direct calculation based on product operator formalism saves much computing time [21]. In such cases, POMA program can be used to predict the evolution process of product operators for a multiple-spin system [43]. When the effects of relaxation, diffusion, and dipolar field in the solution NMR are taken into account, the product operator matrix method of this work can effectively simulate inter-molecular MQCs with scalar couplings for a multiple-spin system.

4. Conclusion

In this paper, a new method is proposed to simulate behaviors of multiple-spin systems with both intra-molecular scalar couplings and inter-molecular dipolar couplings. The method utilizes a combined approach with product operator matrix operators, non-linear Bloch equations, and Monte Carlo simulations. The validity of the method is tested with experiments in sample systems. We demonstrate that the proposed method provides a convenient tool for studying behaviors of complex spin systems under the effects of chemical shift, dipolar field, radiation damping, self-diffusion, and scalar couplings, and with different pulse sequences. NMR spectra produced by complex pulse sequences may be predicted by simulations before experiments are performed. This will reduce experimental time since best experimental conditions can be identified and optimal

parameters can be chosen through simulations. Furthermore, since the cross-peaks in 2D spectra of complex spin systems are in general complicated and crowded, the simulation would be of great help in peak assignment and interpretation in such cases, which is always very difficult from precise theoretical analysis. The potential problems occurred in experiments may also be identified. The simulation method proposed herein is also promising for studying scalar couplings in inter-molecular MQC imaging or the chaotic phenomena produced by the joint effects of dipolar field and radiation damping.

Computational time for simulation increases fourfold every time the number of spins in a spin system increases by one. Fortunately, spin systems usually contain some equivalent spins, which results in certain types of symmetry for the product operator matrix. For example, the number of elements of the product operator matrix for AX_3 spin system is reduced to 5/16 of its original ones when the symmetry is taken into consideration. How to make effective use of properties of symmetry in simulation processes is still an unanswered question. The method presented herein works well for the weakly coupled spin 1/2 system. We are in the process to extend it to strongly coupled spin-1/2 and/or high spin ($I > 1/2$) systems.

Acknowledgments

This work was partially supported by the NNSF of China under Grants 10234070, 10375049 and 10104011, and NIH under Grants NS32024 and NS41048.

References

[1] F. Bloch, Nuclear induction, Phys. Rev. 70 (1946) 460–474.
[2] P.K. Madhu, A. Kumar, Bloch equations revisited: new analytical solutions for the generalized Bloch equations, Concept. Magn. Reson. 9 (1997) 1–12.
[3] H.C. Torrey, Bloch equations with diffusion terms, Phys. Rev. 104 (1956) 563–565.
[4] J. Jeener, Dynamical effects of the dipolar field inhomogeneities in high-resolution NMR: spectral clustering and instabilities, Phys. Rev. Lett. 82 (1999) 1772–1775.
[5] D.E. Rourke, L. Khodarinova, A.A. Karabanov, Two-level systems with relaxation, Phys. Rev. Lett. 92 (1–4) (2004) 163003.
[6] L.A. Stables, R.P. Kennan, A.W. Anderson, J.C. Gore, Density matrix simulations of the effects of J coupling in spin echo and fast spin echo imaging, J. Magn. Reson. 140 (1999) 305–314.
[7] S. Lee, W. Richter, S. Vathyam, W.S. Warren, Quantum treatment of the effects of dipole–dipole interactions in liquid nuclear magnetic resonance, J. Chem. Phys. 105 (1996) 874–900.
[8] W.S. Warren, S.Y. Yang, S. Ahn, Y.Y. Lin, Understanding third-order dipolar effects in solution nuclear magnetic resonance: Hahn echo decays and intermolecular triple-quantum coherences, J. Chem. Phys. 116 (2002) 2075–2084.
[9] J. Jeener, Equivalence between the "classical" and the "Warren" approaches for the effects of long range dipolar couplings in liquid nuclear magnetic resonance, J. Chem. Phys. 112 (2000) 5091–5094.
[10] J. Jeener, A. Vlassenbroek, P. Broekaert, Unified derivation of the dipolar field and relaxation terms in the Bloch-Redfield equations liquid NMR, J. Chem. Phys. 103 (1995) 1309–1332.
[11] Z. Chen, Z.W. Chen, J. Zhong, High-resolution NMR spectra in inhomogeneous fields via IDEAL (intermolecular dipolar-interaction enhanced all lines) method, J. Am. Chem. Soc. 126 (2004) 446–447.
[12] Z. Chen, Z.W. Chen, J. Zhong, Quantitative characterization of intermolecular dipolar interactions of two-component systems in solution nuclear magnetic resonance, J. Chem. Phys. 115 (2001) 10769–10779.
[13] Y.Y. Lin, N. Lisitza, S.D. Ahn, W.S. Warren, Resurrection of crushed magnetization and chaotic dynamics in solution NMR spectroscopy, Science 290 (2000) 118–121.
[14] L.S. Bouchard, R.R. Rizi, W.S. Warren, Magnetization structure contrast based on intermolecular multiple-quantum coherences, Magn. Reson. Med. 48 (2002) 973–979.
[15] C. Ramanathan, R. Bowtell, Dynamics of the nuclear magnetic resonance COSY-revamped by asymmetric z-gradients (CRAZED) experiment, J. Chem. Phys. 114 (2001) 10854–10859.
[16] G. Deville, M. Bernier, J.M. Delrieux, NMR multiple echoes observed in solid ^{3}He, Phys. Rev. B 19 (1979) 5666–5689.
[17] S. Garrett-Roe, W.S. Warren, Numerical studies of intermolecular multiple quantum coherences: High-resolution NMR in inhomogeneous fields and contrast enhancement in MRI, J. Magn. Reson. 146 (2000) 1–13.
[18] W.S. Price, Pulsed-field gradient nuclear magnetic resonance as a tool for studying translational diffusion. 1. Basic theory, Concept. Magn. Reson. 9 (1997) 299–336.
[19] J. Jeener, Macroscopic molecular diffusion in liquid NMR, revisited, Concept. Magn. Reson. 14 (2002) 79–88.
[20] W.H. Press, S.A. Teukolsky, W.T. Vetterling, B.P. Flannery, Numerical Recipes in C, second ed., Cambridge University Press, New York, 1992.
[21] S. Ahn, W.S. Warren, S. Lee, Quantum treatment of intermolecular multiple-quantum coherences with intramolecular J coupling in solution NMR, J. Magn. Reson. 128 (1997) 114–129.
[22] M. Edén, Computer simulations in solid-state NMR. I. Spin dynamics theory, Concept. Magn. Reson. 17 A (2003) 117–154.
[23] J. Jeener, Collective effects in liquid NMR: dipolar field and radiation damping, in: D.M. Grant, R.K. Harris (Eds.), Encyclopedia of Nuclear Magnetic Resonance, vol. 9, Wiley, New York, 2002, pp. 642–679.
[24] W.B. Blanton, BlochLib: a fast NMR C++ tool kitH, J. Magn. Reson. 162 (2003) 269–283.
[25] M.L. Liu, X. Zhang, Multiple-quantum J-resolved NMR spectroscopy (MQ-JRES): measurement of multiple-quantum relaxation rates and relative signs of spin coupling constants, J. Magn. Reson. 146 (2000) 277–282.
[26] O.W. Sørensen, G.W. Eich, M.H. Levitt, G. Bodenhausen, R.R. Ernst, Product operator-formalism for the description of NMR pulse experiments, Prog. NMR Spectrosc. 16 (1983) 163–192.
[27] H. Hagslatt, B. Jonsson, M. Nyden, O. Soderman, Predictions of pulsed field gradient NMR echo-decays for molecules diffusing in various restrictive geometries: simulations of diffusion propagators based on a finite element method, J. Magn. Reson. 161 (2003) 138–147.
[28] C.L. Chin, F.W. Wehrli, S.N. Hwang, M. Takahashi, D.B. Hackney, Biexponential diffusion attenuation in the rat spinal cord: computer simulations based on anatomic images of axonal architectureH, Magn. Reson. Med. 47 (2002) 455–460.
[29] M.H. Blees, The effect of finite duration of gradient pulses on the pulsed field gradient NMR method for studying restricted diffusion, J. Magn. Reson. A 109 (1994) 203–209.
[30] J.M. Hammersley, D.C. Handscomb, Monte Carlo Methods, Wiley, London, 1964.

[31] G.X. Lin, Z. Chen, J. Zhong, D.H. Lin, X.L. Liao, A novel propagator approach for NMR signal attenuation due to anisotropic diffusion under various magnetic field gradients, Chem. Phys. Lett. 335 (2001) 249–256.
[32] L. Ardelean, E. Kossel, R. Kimmich, Attenuation of homo- and heteronuclear multiple spin echoes by diffusion, J. Chem. Phys. 114 (2001) 8520–8529.
[33] Z. Chen, Z.W. Chen, J.H. Zhong, Observation and characterization of intermolecular homonuclear single-quantum coherences in liquid nuclear magnetic resonance, J. Chem. Phys. 117 (2002) 8426–8435.
[34] S.M. Brown, P.N. Sen, D.G. Cory, Nuclear magnetic resonance scattering across interfaces via the dipolar demagnetizing field, J. Chem. Phys. 116 (2002) 295–301.
[35] D. Zax, A. Pines, Study of anisotropic diffusion of oriented molecules by multiple quantum spin echoes, J. Chem. Phys. 78 (1983) 6333–6334.
[36] M.L. Liu, X.A. Mao, Enhanced effect of magnetic field gradients using multiple quantum NMR spectroscopy applied to self-diffusion coefficient measurement, Mol. Phys. 96 (1998) 913–920.
[37] S.K. Zheng, Z. Chen, Z.W. Chen, J. Zhong, Direct measurement of transverse relaxation time of intermolecular multiple quantum coherences in NMR, Chin. Phys. 10 (2001) 558–563.
[38] J. Zhong, Z. Chen, S.K. Zheng, S.D. Kennedy, Theoretical and experimental characterization of NMR transverse relaxation process related to intermolecular dipolar interactions, Chem. Phys. Lett. 350 (2001) 260–268.
[39] S. Ahn, S. Lee, W.S. Warren, The competition between intramolecular J couplings, radiation damping, and intermolecular dipolar couplings in two-dimensional solution nuclear magnetic resonance, Mol. Phys. 95 (1998) 769–785.
[40] F. Fasanoa, S. Capuanib, G.E. Hagberga, T. Brancab, I. Indovinaa, A. Castriota-Scanderbega, B. Maravigliac, Intermolecular double quantum coherences (iDQC) and diffusion-weighted imaging (DWI) imaging of the human brain at 1.5 T, Magn. Reson. Imag. 21 (2003) 1151–1157.
[41] J.P. Marques, R. Bowtell, Optimizing the sequence parameters for double-quantum CRAZED imaging, Magn. Reson. Med. 51 (2004) 148–157.
[42] T. Hou, Z. Chen, D.W. Hwang, J.H. Zhong, L.P. Hwang, Intermolecular double-quantum coherence MR microimaging of pig tail with unique image contrast, Magn. Reson. Imag. 22 (2004) 543–550.
[43] P. Güntert, N. Schaefer, G. Otting, K. Wüthrich, POMA: a complete mathematica implementation of the NMR product-operator formalism, J. Magn. Reson. A 101 (1993) 103–105.